eXPRESS Polymer Letters Vol.13, No.7 (2019) 632–641
Available online at www.expresspolymlett.com
https://doi.org/10.3144/expresspolymlett.2019.53

3D scanning probe nanotomography of tissue spheroid fibroblasts interacting with electrospun polyurethane scaffold

A. E. Efimov[1,2], O. I. Agapova[1], L. A. Safonova[1,3], M. M. Bobrova[1,3], V. A. Parfenov[4], E. V. Koudan[4], F. D. A .S. Pereira[4], E. A. Bulanova[4], V. A. Mironov[4,5], I. I. Agapov[1]*

[1]Laboratory of Bionanotechnology, Academician V.I. Shumakov National Medical Research Center of Transplantology and Artificial Organs, Ministry of Health of the Russian Federation, 123182 Moscow, Russian Federation.
[2]SNOTRA LLC., 121205 Moscow, Russian Federation.
[3]Bioengineering Department, Biological Faculty, Lomonosov Moscow State University,119991 Moscow, Russian Federation.
[4]Private Institution Laboratory for Biotechnological Research '3D Bioprinting Solutions', 115409 Moscow, Russian Federation.
[5]Institute for Regenerative Medicine, I.M. Sechenov First Moscow State Medical University, 119991 Moscow, Russian Federation

Received 12 December 2018; accepted in revised form 18 February 2019

Abstract. We present a 3D study of nanostructural features of a bioprinted tissue spheroid interacting with polyurethane dual-scale biocompatible scaffold manufactured by three-dimensional printing and electrospinning. Three-dimensional analysis of fibroblasts interacting with electrospun polyurethane fibers was conducted using scanning probe nanotomography with an experimental setup combining ultramicrotome and a scanning probe microscope. Three-dimensional reconstruction demonstrates direct visualization of cell membrane protrusions and coherent cell-fiber interfaces, the formation of which is a prerequisite for an efficient tissue engineered implant. Analysis of obtained 3D data allows for quantitative calculation of the important morphological parameters of adhered cells, scaffolds, and cell-scaffold interfaces. The proposed method may be successfully applied to investigate 3D cell-scaffold constructs at nanoscale.

Keywords: *biocompatible polymers, electrospinning, nanotomography, tissue spheroids, bioprinting*

1. Introduction

Emerging additive technologies such as 3D printing and electrospinning have become indispensable in tissue engineering and regenerative medicine. These technologies enable such tasks as creation of implantable 3D scaffolds with suitable morphology, mechanical properties, and biocompatibility that allows culturing of essential cells and tissue fragments [1, 2]. Such morphological characteristics of scaffolds as volume porosity, pore dimensions, interconnectivity of porous systems, and surface area to volume ratio are crucial for sufficient cell adhesion and proliferation and consequent ingrowth and vascularization of tissue [3].

Electrospinning is based on the electric field induced stretching of ultrathin fibers from the solution and enables production of 2D and 3D polymer microfibrous structures. These structures have varied architecture and controlled fiber diameters ranging from several nanometer to 10 microns [4–7]. It is widely used to fabricate porous scaffolds for cell carriers from various biopolymer materials.

*Corresponding author, e-mail: antefimov@gmail.com

After the scaffold is manufactured, the next step needed for fabrication of a tissue-engineered construct is effective deposition of cells or tissue fragments onto the scaffold. One of the most prospective and rapidly developing methods for deposition of biological material onto carriers is 3D bioprinting. This technique is most effectively realized by printing with cell aggregates such as tissue spheroids (which usually have a diameter of several hundred microns and may contain tens of thousands of living cells) in accordance with a preset digital 3D model [8–11]. The spreading and fusion of spheroids in the porous scaffold leads to the formation of continuous bio-artificial tissue.

In previous work [12], we described the technology of fabrication and analysis of the 3D nanostructure of dual-scale scaffolds produced by 3D printing and electrospinning from biocompatible polyurethane. Such dual-scale scaffolds may serve as a universal micro- and nanostructural platform for bioprinted tissue-engineered constructs that correspond to internal organs [13, 14].

We also have explored nanostructural features of human fibroblast spheroids interacting with such dual-scale polyurethane scaffold by means of scanning electron microscopy (SEM) [15] and 2D atomic force microscopy (AFM) [16], proving high biocompatibility of the electrospun scaffold. However, developing of effective tissue-engineered constructs based on three-dimensional biocompatible scaffolds requires elaborate 3D analysis and control of the scaffold architecture and characteristics of cell-scaffold interactions on micro- and nanoscale. Developing proper 3D imaging approaches for tissue engineering applications is challenging in terms of achievable resolution, contrast, imaging depth, and possible sample damage issues [17].

Such 3D microscopy techniques as focused ion beam (FIB) -scanning electron microscopy (SEM) [18, 19] and X-ray nanotomography with Zernike phase contrast [20] provide comprehensive 3D evaluation of scaffolds and cells-scaffold interaction including analysis of cells grown on electrospun PLGA scaffolds and corresponding cell-scaffold interfaces [19, 20]. Zernike method of X-ray phase contrast imaging maybe effectively used for generation of high-contrast images which allow distinguishing of cell and scaffold details. However, typically this method gives rise to halo artifacts at the edges of features, arising from diffracted X-rays from the sample, which pass through the phase ring, having low angular deviation [21]. These artifacts can make image segmentation for 3D reconstruction of cell-scaffold system morphology more difficult. They may be almost totally removed with use of proper deconvolution image filtering procedure described in [20], but it leads to loss of effective resolution – in that case from 150 down to 320 nm.

A resolution of 50 nm has been achieved during X-ray nanotomography of bone tissue, albeit with the sample dimensions limited to 50 μm or less, which is not suitable for analysis of most bio-artificial cell-scaffold or tissue-scaffold systems [22].

FIB/SEM technique may provide impressive results in terms of resolution, but it may also cause unfavorable structural changes in biological and polymer samples because of electron and ion radiation damage [23]. Restrictions of X-ray and SEM/FIB tomographies are unsuitable in many cases for studies of cell-scaffold systems, and development of complementary 3D microscopy techniques remains necessary for more comprehensive analyses [24].

In the present work, we demonstrate an example of 3D nanoscale analysis of a cell-scaffold system using an alternative analytical technology, scanning probe nanotomography (SPNT), which is a combination of methods of serial sectioning by ultramicrotomy and study of the sample blockface surface by scanning probe microscopy (SPM) after each sectioning [25–27]. This technology enables users to obtain a series of SPM images of sectioned cells and scaffold fiber surfaces and conduct 3D reconstruction of the structures by integrating obtained serial SPM images. Here, we present a 3D study of interactions of electrospun polyurethane scaffold with cells of bioprinted tissue spheroids produced from primary human fibroblasts.

2. Experimental

2.1. Manufacturing of dual-scale polyurethane scaffold samples

Scaffold samples were manufactured using biocompatible polyurethane (PU), officially approved for clinical use in the United States (EG-85A, Lubrizol Corp., Wickliffe, OH, USA; courtesy of prof. Xuejun Wen, Virginia Commonwealth University, Richmond, VA, USA). Dual-scale scaffolds measuring 10×10×1.3 mm were produced by combining 3D-printing and electrospinning techniques.

Three-dimensional printing was conducted using 3D printer Duplicator i3 (Wanhao 3D Printer, Jinhua,

China). The following PU 3D-printing parameters were applied: nozzle diameter – 0.4 mm; thickness of deposited layer – 0.3 mm; platform temperature – +50 °C; nozzle temperature – +210/215 °C; working velocity in the printing plane – 10 mm/s. Fabricated scaffold samples comprise three layers of PU stripe grids with direction of stripes in each layer perpendicular to neighboring layers, stripe cross-section is 0.4 mm×0.4 mm and grid period is 0.8 mm.

PU fibers were deposited on 3D-printed PU grid scaffold by electrospinning performed on Professional Lab Device (Yflow S.D., Malaga, Spain). PU for electrospinning was dissolved with 17% concentration in dissolvent containing 60% of tetrahydrofuran (Component-Reactiv LLC., Moscow, Russia) and 40% of dimethylformamide (DMF, Sigma-Aldrich, St. Louis, MO, USA) by volume. The electrospinning process was conducted using the following parameters: voltage on the needle – 20 kV; distance from needle tip to collector – 20 cm; needle diameter 0.6 mm; polymer supply rate – 1.3 ml/h [12].

2.2. Fabrication and bioprinting of tissue spheroids

Tissue spheroids were fabricated from primary human fibroblasts using 96-well plates with non-adhesive coating (Corning Corp., Corning, NY, USA, cat. № 4520). Primary human fibroblasts (Lonza GmbH, Cologne, Germany, cat. № CC-2511) were cultivated at 37 °C in a humidified atmosphere with 5% CO_2 in Dulbecco's modified Eagle's medium (DMEM, Gibco, Thermo Fisher Scientific, Waltham, MA, USA, cat. № 12491-015) containing 10% fetal bovine serum (Gibco, Thermo Fisher Scientific, Waltham, MA, USA cat. № 16000-044) supplemented 1 mM l-glutamine (Paneco, Moscow, Russian Federation, cat. № F032) and antibiotic/antimycotic mixture (Gibco, Thermo Fisher Scientific, Waltham, MA, USA, cat. № 15240–062). Cell suspension with concentration of $5.5 \cdot 10^4$ cell/ml was produced from initial primary human fibroblast culture. One hundred microliters of cell suspension was placed in each well of the plates with non-adhesive coating. Plates with forming spheroids were incubated at 37 °C in a humidified atmosphere with 5% CO_2 for 72 hours. Spheroids obtained were placed on the surface of electrospun polyurethane scaffold using the original FABION 3D multifunctional bioprinter (3D Bioprinting Solutions, Moscow, Russia) with a conic-like pipette that enables users to place individual tissue spheroids on the substrate surface with high precision according to a preset digital model [15].

2.3. Scanning electron microscopy

For SEM studies, the samples of scaffolds with adhered fibroblast spheroids (spreading period – 48 hours) were washed in PBS buffer twice for 30 minutes each, then dehydrated through an ascending series of ethanol solutions: 30% – 30 minutes, 50% – 30 minutes, 70% – 30 minutes, 80% – 30 minutes, 96% – 2 times for 30 minutes each, 100% 2 times for 30 minutes each. The critical point drying process was conducted according to a standard procedure using CO_2 as a working fluid and 100% ethanol as an intermediate fluid with HCP-2 setup (Hitachi, Tokyo, Japan). To avoid surface charge while imaging the sample, a holder with the samples was coated by ion sputtering in an Ar atmosphere (with pressure of ~ 0.1 mm Hg) with a ~20 nm thick Au-Pd layer. SEM study of the samples was performed using SEM JSM -6510LV (JEOL, Tokyo, Japan) with an accelerating voltage of 30 kV, operating distance 20 mm, and tilt of the sample table of 30 °.

2.4. Scanning probe nanotomography

For study of 3D micro- and nanostructure of cells and scaffolds, we used NTEGRA-Tomo system (NT-MDT Spectrum Instruments Co., Moscow, Russia), which comprises a scanning probe microscope combined with Leica EM UC6 ultramicrotome (Leica Microsystems GmbH, Vienna, Austria) [25]. The maximal scanning surface area is 95.0×95.0 μm.

For SPNT studies, the samples of scaffolds with adhered fibroblast spheroids (spreading period – 48 hours) were dehydrated similarly to the SEM-preparation procedure and embedded in epoxy embedding media (Sigma-Aldrich, St. Louis, MO, USA, Cat. № 45345). Embedding and polymerization of epoxy embedding media was conducted for 72 hours at temperature of 50 °C.

Samples were sectioned using an Ultra sonic 35 diamond knife (Diatome AG, Nidau, Switzerland) with 3.0 mm blade width. Section thickness was 80 nm (setting). SPM measurements were performed in the semicontact mode at scanning rate of 1 Hz using silicon cantilever tips ETALON HA_HR (NT-MDT Spectrum Instruments Co., Moscow, Russia) with resonant frequency of 390 kHz and a tip radius smaller than 10 nm. Preliminary image processing was performed with Nova ImageAnalysis 1.0.26.1443

software (NT-MDT Spectrum Instruments Co., Moscow, Russia). 3D reconstruction and visualization were conducted using Image Pro AMS 6.0 software package with 3DConstructor option (MediaCybernetics Inc., Rockville, MD, USA).

3. Results and discussion

Tissue spheroids were deposited to the surface of electrospun PU dual-scale scaffold by a FABION 3D multifunctional bioprinter (3D Bioprinting Solutions, Moscow, Russia) and fixed 48 hours after the deposition. After fixation and sample processing, these samples were investigated using SEM and SPNT. An illustrative schema of the sample fabrication steps is shown in Figure 1.

Figure 2a shows the SEM image of a single tissue spheroid on the electrospun PU scaffold surface 48 hours after bioprinting. The SEM image demonstrates that some individual fibroblasts had migrated a significant distance from the spheroid (up to several hundred microns) but the spheroid retained its shape. This is consistent with results of other studies, reporting that tissue spheroids on electrospun scaffolds may exhibit significant flattening only after 4 days and total spreading after 7 days after seeding, depending on the substrate and cell characteristics [9, 10, 15].

Figure 2b shows SEM image of individual migrating fibroblast outside of the spheroid adhered to electrospun PU microfibers of the scaffold. Obtained SEM data enabled us also to analyze some parameters of PU fiber scaffold itself. We have determined that the mean diameter of microfibers is 1.64±0.43 μm (n = 70), with dimensions of pores between microfibers ranging from 5 to 15 μm. However, analysis of 3D data is necessary to determine volume porosity and surface area to volume ratio of the scaffold, which cannot be derived from 2D SEM images.

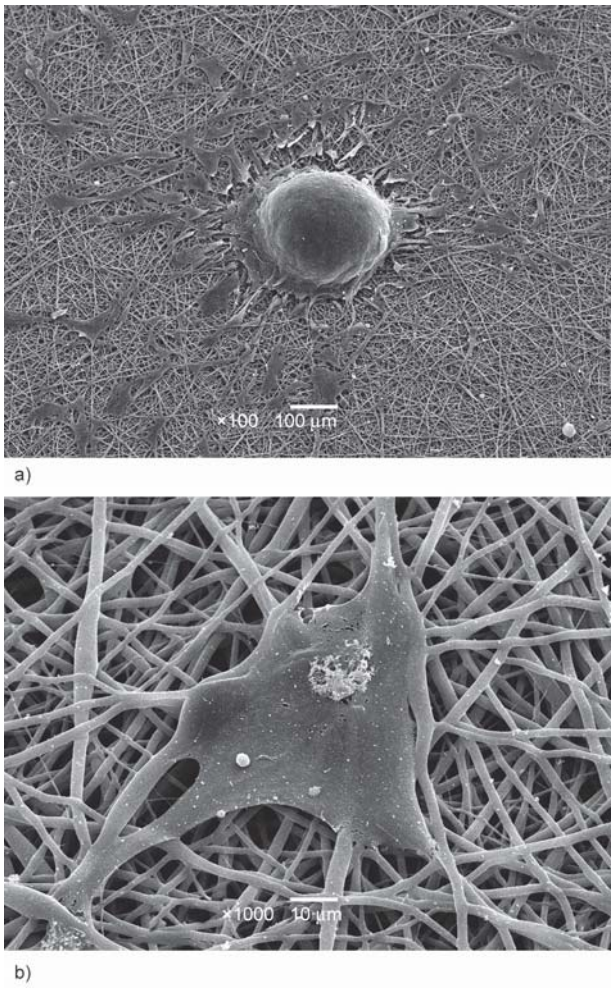

Figure 2. (a) SEM image of a tissue spheroid bioprinted on the surface of PU scaffold. Time after bioprinting – 48 h, magnification – ×100, scale bar 100 μm; (b) SEM image of individual migrated fibroblast cell outside of the spheroid, adhered to PU fibers. Time after bioprinting – 48 h, magnification – ×1000, scale bar 10 μm.

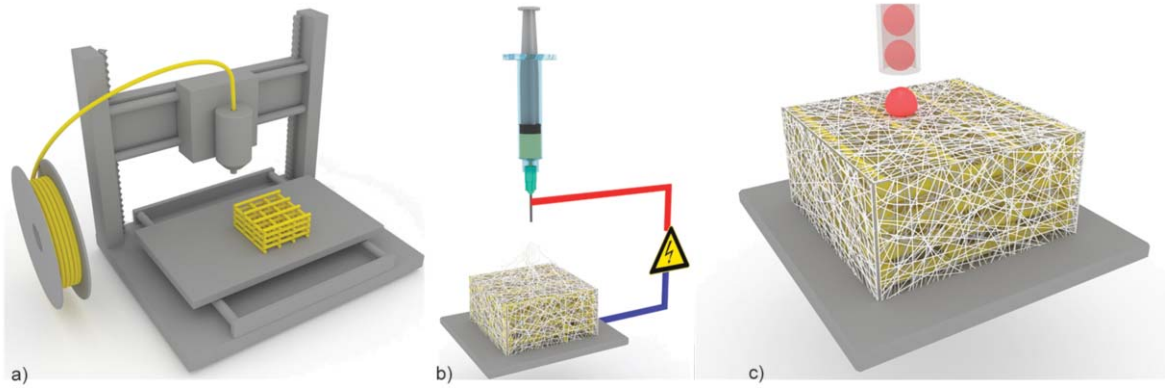

Figure 1. Scheme of the sample fabrication. (a) 3D-printing of PU scaffold in a fused deposition modelling 3D printer; (b) Electrospinning of PU microfibers on the scaffold; (c) Deposition of cellular spheroids on the surface of electrospun microfibrous PU scaffold using bioprinter.

Figure 3 shows phase SPM image (32.0×32.0 μm^2) of the ultramicrotomed sample surface in the area outside of the spheroid. The sample was sectioned perpendicularly to the plane of 3D printed scaffold. Here we can see cross-sections of the electrospun scaffold fibers in the right part of the image, having circular or elongated shapes, and individual migrating cell adhered in some points to the fibers with formation

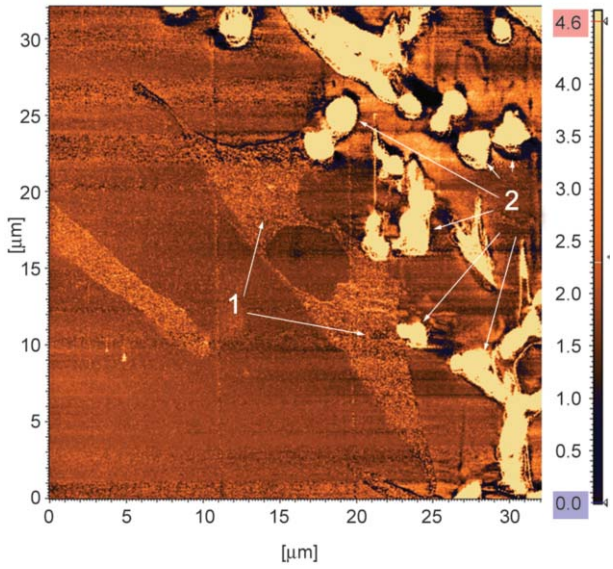

Figure 3. SPM image of the ultramicrotomed sample surface in the area outside of the spheroid containing individual migrating cell (1) adhered to the PU fibers (2). Phase imaging mode, scan size 32.0×32.0 μm^2.

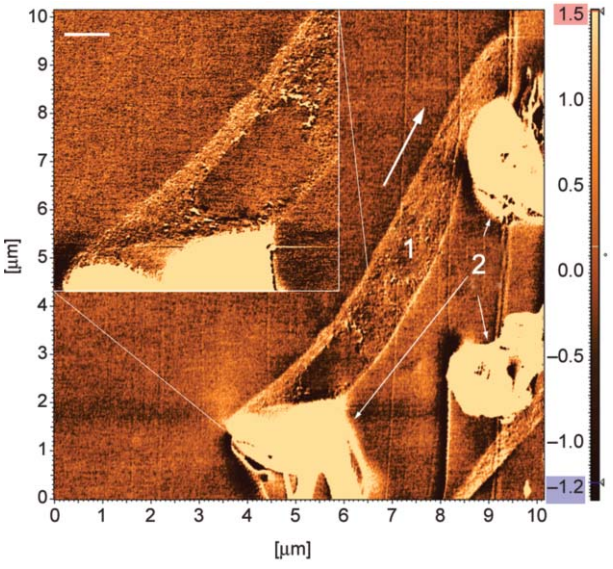

Figure 4. SPM image of the ultramicrotomed sample surface in the area outside of the spheroid containing individual migrating cell (1) adhered to the fibers (2). The arrow indicates the direction of the cell migration along the scaffold plane. Phase imaging mode, scan size 10.0×10.0 μm^2. Scale bar in the inset: 500 nm.

of typical membrane protrusions. Due to sufficiently different viscoelastic properties, PU fibers demonstrate high phase contrast on SPM images compared with the surrounding epoxy and cell material and may be clearly distinguished.

Figure 4 shows another image of smaller migrating cell contacting the fibers via elongated thinner membrane protrusions with thickness of 100–200 nm. This cell is located approximately at 160 μm distance from the spheroid border along the scaffold. The arrow indicates the direction of cell migration along the scaffold surface (if we are assuming that the cells migrate in the plane of the scaffold away from the spheroid); the image shows that the imaged cell-fiber contacts in the inset correspond to the rear part of the cell, which is about to detach from the fiber. Nanoscale organization of the plasma membrane protrusions underlies cell progression and thus distribution of cells in the scaffold and tissue ingrowth [28, 29]. Therefore, 3D analysis of their nanomorphology is indispensable to understand cell-scaffold dynamic interactions.

We performed SPNT 3D reconstruction of a cell on the fibers depicted in Figure 3, collecting the series of 23 consequent SPM image sets. Each SPM image set was acquired after the previous 150 nm ultramicrotome section of the sample surface and comprised a 512×512 pixel topography and phase images obtained simultaneously from the same 32.0×32.0 μm^2 area. Binarization and segmentation of PU fiber images by thresholding was straightforward due to their high contrast on SPM phase images. Segmentation of cell images was performed manually. In this dataset, topography SPM images offered a more comprehensive contrast in the cell ultrastructure, so they were segmented and used for 3D reconstruction stitched with corresponding phase images of PU fibers.

Three-dimensional reconstruction of segmented and stitched images was conducted using Image Pro AMS 6.0 with 3DConstructor option (Media Cybernetics Inc., Rockville, MD, USA). The resulting 3D reconstruction visualizations viewed from two different angles are presented in Figure 5. In these images, we can directly detect coherent interfaces between fibroblast and electrospun PU fibers, marked in Figure 5b.

Obtained 3D data enabled us to calculate quantitative morphological characteristics of the cell and cell-fiber interfaces. The measured average thickness of the cell perpendicular to the scaffold plane is

4.5 μm. The average area of the cell cross-section perpendicular to the scaffold plane is 116.4±22.4 μm^2, while that of the perimeter of the cell cross-section is 90.6±11.6 μm, calculated as average ratio of reconstructed cell surface area to the depth. These parameters significantly influence diffusion properties of cellular cytoplasm, which determines the cell's biological activity [30]. The average perimeter length of cell contact with the scaffold fibers in the same plane is 9.9±2.2 μm, so we may conclude that only approximately 11% of cell surface by area is in contact with the fibers and forming coherent cell-fiber interfaces.

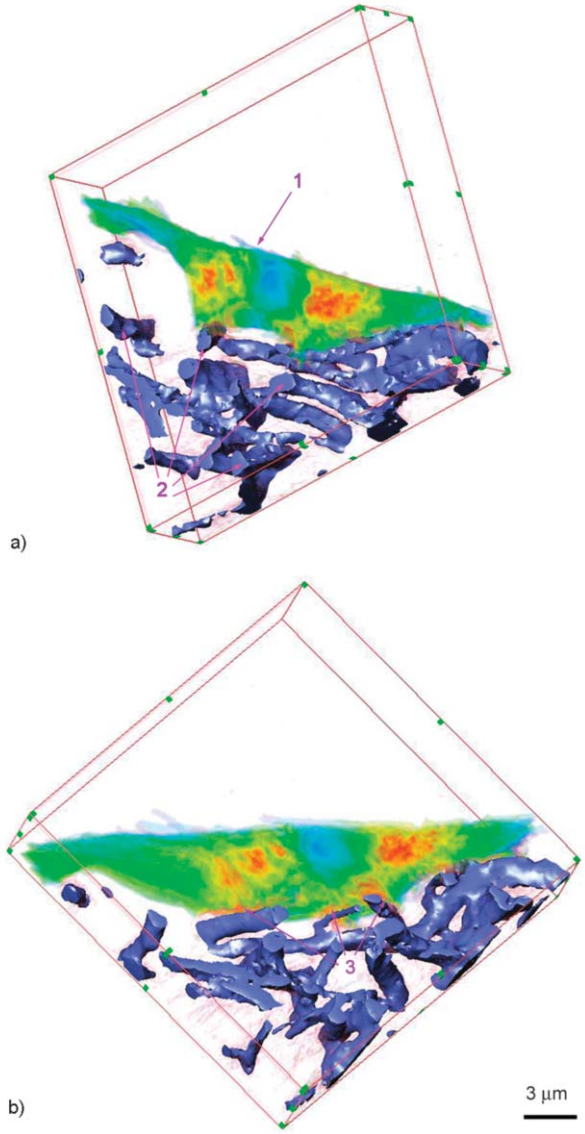

Figure 5. (a) SPNT 3D reconstruction of the fibroblast (1) imaged in Figure 3 and surrounding electrospun PU fibers (2). Twenty-three 150 nm-thick sections, reconstructed volume 32.0×32.0×3.3 μm; (b) Another foreshortening of the same 3D reconstruction showing coherent interfaces (3) formed between fibroblast and fibers.

Mathematical analysis of the reconstructed cell surfaces allowed calculation of the 3D morphological parameters of these surfaces on the nanoscale. We analyzed such parameters of cell surfaces as average roughness (R_a) and effective surface area (σ) [31]. It is worth noting, that these 3D morphological parameters could not be directly assessed from 2D microscopy techniques data (SEM and AFM of ultramicrotomed surface) which were used in [16].

The obtained average roughness R_a of the reconstructed cell membrane surface was 24.4±2.2 nm. The roughness of the cell membrane surface is an important cytological parameter involved in several cellular mechanisms including motility, adhesion, and intracellular contact [32–34]. It may serve as a sensitive indicator of the cell's health [35–37].

In addition to roughness, the effective surface area of the membrane is also important in determining the condition and biological activity of the cell [38]. This parameter determines the degree of surface development. Here, we calculate σ as the unitless ratio of reconstructed surface area to the area of its two-dimensional projection on the plane. Area of reconstructed 3D surface is calculated using a triangulation method, as a sum of elementary cell areas among adjacent surface points of the surface. Details of the methods used to calculate σ and R_a parameters are given in [31]. The calculated effective area for reconstructed cell surface was 1.153±0.01.

Similarly, analysis of PU fibers images allowed us to determine three-dimensional parameters of the electrospun scaffold. We determined that the fibers occupy 23.5% of the total scaffold volume, so the volume porosity of the scaffold may be estimated to be 76.5%. The mean surface area to volume ratio was estimated to be 4.18±0.54 μm^{-1}. Obtained quantitative morphological parameters of adhered cells and the PU fiber scaffold are presented in Table 1.

Table 1. Quantitative morphological parameters of cells and scaffold obtained from SPNT 3D data.

Cell morphological parameters		
Cross-section area	[μm^2]	116.4±22.4
Cross-section perimeter	[μm]	90.6±11.6
Surface roughness (R_a)	[nm]	24.4±2.2
Effective surface area (σ)		1.153±0.01
Scaffold morphological parameters		
Microfiber diameter	[μm]	1.64±0.43
Volume porosity	[%]	76.5
surface area-to-volume ratio	[μm^{-1}]	4.18±0.54

Another examples of a blockface SPM phase image (25.0×25.0 μm^2) containing several cells and PU fibers and corresponding 3D SPNT reconstruction (twelve 150 nm-thick sections) are presented in Figure 6. Here, we can also see elongations of the cell membrane connecting with the fibers, with coherent interfaces forming.

Previous studies demonstrated that fibroblasts adhered to electrospun scaffolds form focal adhesion clusters (FAC) where the cell interacts with the fibers [39, 40]. In Figures 3 and 5, we can see the cell membrane protrusions that semi-envelope the fibers, so we can suppose formation of FACs there. Such behavior is considered typical for fibroblasts, although cells of other types may demonstrate different modalities of cell-fiber interaction. For example, a recent 3D microscopy study that used SPNT showed that neonatal rat cardiomyocytes tend to totally envelop the nanofibers, forming a sheath-like structure [41]. However, no SPNT 3D-reconstruction of fibroblasts interacting with electrospun microfibers has been carried out before.

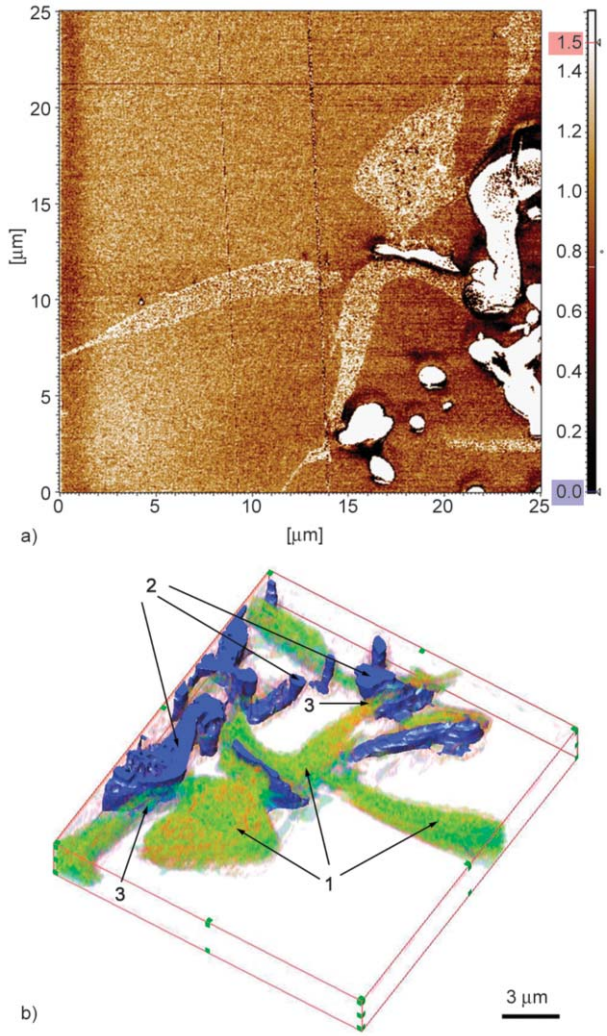

Figure 6. SPM phase image, scan size 25.0×25.0 μm^2 (a) and corresponding SPNT 3D reconstruction (b) of reconstructed volume 25.0×25.0×1.8 μm (twelve sections 150 nm-thick sections), showing cells (1) connecting with the PU fibers (2) by elongations (3) of the cell membrane, with coherent interfaces forming.

Observed cell-scaffold interaction features show that the PU electrospun scaffold studied may be suitable for both adhesion and migration of fibroblast cells [42–44]. The presented technique of 3D micro- and nanostructural investigation of cell-scaffold interaction with SPNT allows for adequate qualitative and quantitative analysis of morphological interaction parameters and overcomes the drawbacks of FIB/SEM and X-ray nanotomography methods such as radiation damage, low contrast, and resolution issues.

Applying the SPNT technique for *in vitro* studies of bio-artificial constructs may help to make comprehensive prognosis of *in vivo* behavior of the tissue-engineered scaffold implant. High-resolution SPM imaging readily enables users to study morphological features of the cells, such as filopodia and lamellipodia with resolution of several tens of nanometers, limited by the pixel physical dimensions and SPM tip sharpness. Depth resolution of the technique is determined by minimal reproducible ultramicrotome section thickness, with the achievable level of 20 nm [25, 26]. The most limiting factor for acquisition of sufficient area high-resolution images, which require increasing number of pixels, and for increasing the number of thinner sections for tomographic reconstruction is therefore the speed of SPM measurements. However, it is not a principal limitation because high-speed SPM technical approaches are extensively developing now [45] and may also be implemented for SPNT measurements, which will improve the technology's usefulness for high resolution analysis of 3D structures of tissue-engineered constructs in larger volumes. Another direction of further development of SPNT technology is integration with high-resolution correlative optical microscopy and spectroscopy [46, 47], which will enable users to conduct correlative studies of nanoscale morphology and distribution of specific fluorescent markers by labeling dynamic focal adhesion sites associated with migrating cells. Considering further developments of the technique, it may become a method of choice for nanostructural analysis of 3D bioengineered systems.

4. Conclusions

In this paper, we present the 3D SPNT study of primary human fibroblast from bioprinted tissue spheroids interacting with polyurethane dual-scale biocompatible scaffold manufactured by three-dimensional printing and electrospinning. We have demonstrated that application of SPNT technique allows for direct visualization of the 3D structures of cells, fibrous scaffolds, and features of cell-scaffold contacts with resolution of at least 60 nm in sectioning planes and 150 nm in depth. Our study has proved the formation of coherent interfaces between fibroblasts and electrospun PU fibers. Analysis of obtained 3D data allows for quantitative calculation of important morphological parameters of adhered cells, scaffolds, and cell-scaffold interfaces such as mean diameter of microfibers, effective volume scaffold porosity and pore dimensions, mean scaffold surface area to volume ratio, cell dimensions, volume and surface area of cells, roughness of cell surface, and surface areas of cell-fiber coherent interfaces.

Considering these results, we may conclude that the use of dual-scale bioprinted tissue-engineered construct fabricated by bioprinted tissue spheroids on the developed scaffold might significantly improve the efficacy of tissue regeneration upon its implantation. The demonstrated method of studying 3D cell-scaffold interfaces can provide new insights into interactions between cells or tissues and cell scaffolds or biopolymer implants.

Acknowledgements

This work was supported by a grant from the Russian Scientific Foundation (project no. 17-75-10098). The datasets generated and/or analyzed during the current study are available from the corresponding author on reasonable request.

References

[1] Dvir T., Timko B. P., Kohane D. S., Langer R.: Nanotechnological strategies for engineering complex tissues. Nature Nanotechnology, **6**, 13–22 (2011). https://doi.org/10.1038/nnano.2010.246

[2] Chan B. P., Leong K. W.: Scaffolding in tissue engineering: General approaches and tissue-specific considerations. European Spine Journal, **17**, 467–479 (2008). https://doi.org/10.1007/s00586-008-0745-3

[3] Costantini M., Colosi C., Mozetic P., Jaroszewicz J., Tosato A., Rainer A., Trombetta M., Święszkowski W., Dentini M., Barbetta A.: Correlation between porous texture and cell seeding efficiency of gas foaming and microfluidic foaming scaffolds. Materials Science and Engineering: C, **62**, 668–677 (2016). https://doi.org/10.1016/j.msec.2016.02.010

[4] Li D., Xia Y.: Electrospinning of nanofibers: Reinventing the wheel? Advanced materials, **16**, 1151–1170 (2004). https://doi.org/10.1002/adma.200400719

[5] Teo W. E., Ramakrishna S.: A review on electrospinning design and nanofibre assemblies. Nanotechnology, **17**, 89–106 (2006). https://doi.org/10.1088/0957-4484/17/14/R01

[6] Kai D., Liow S. S., Loh X. J.: Biodegradable polymers for electrospinning: Towards biomedical applications. Materials Science and Engineering: C, **45**, 659–670 (2014). https://doi.org/10.1016/j.msec.2014.04.051

[7] Jin L., Wang T., Zhu M-L., Leach M. K., Naim Y. I., Corey J. M., Feng Z-Q., Jiang Q.: Electrospun fibers and tissue engineering. Journal of Biomedical Nanotechnology, **8**, 1–-9 (2012). https://doi.org/10.1166/jbn.2012.1360

[8] Lin H., Li Q., Lei Y.: Three-dimensional tissues using human pluripotent stem cell spheroids as biofabrication building blocks. Biofabrication, **9**, 025007/1–025007/16 (2017). https://doi.org/10.1088/1758-5090/aa663b

[9] Chua K-N., Lim W-S., Zhang P., Lu H., Wen J., Ramakrishna S., Leong K. W., Mao H-Q.: Stable immobilization of rat hepatocyte spheroids on galactosylated nanofiber scaffold. Biomaterials, **26**, 2537–2547 (2005). https://doi.org/10.1016/j.biomaterials.2004.07.040

[10] Beachley V., Kasyanov V., Nagy-Mehesz A., Norris R., Ozolanta I., Kalejs M., Stradis P., Baptista L., da Silva K., Grainjero J., Wen X., Mironov V.: The fusion of tissue spheroids attached to pre-stretched electrospun polyurethane scaffolds. Journal of Tissue Engineering, **5**, 8–15 (2014). https://doi.org/10.1177/2041731414556561

[11] Dababneh A. B., Ozbolat I. T.: Bioprinting technology: A current state-of-the-art review. Journal of Manufacturing Science and Engineering, **136**, 061016/1–061016/11 (2014). https://doi.org/10.1115/1.4028512

[12] Efimov A. E., Agapova O. I., Parfenov V. A., Pereira F. D. A. S., Bulanova E. A., Mironov V. A., Agapov I. I.: Investigating the micro- and nanostructure of microfibrous biocompatible polyurethane scaffold by scanning probe nanotomography. Nanotechnologies in Russia, **10**, 925–929 (2015). https://doi.org/10.1134/S1995078015060038

[13] Ozbolat I. T., Yu Y.: Bioprinting toward organ fabrication: Challenges and future trends. IEEE Transactions on Biomedical Engineering, **60**, 691–699 (2013). https://doi.org/10.1109/tbme.2013.2243912

[14] Chang C. C., Boland E. D., Williams S. K., Hoying J. B.: Direct-write bioprinting three-dimensional biohybrid systems for future regenerative therapies. Journal of Biomedical Materials Research Part B: Applied Biomaterials, **98B**, 160–170 (2011). https://doi.org/10.1002/jbm.b.31831

[15] Mironov V., Khesuani Y. D., Bulanova E. A., Koudan E. V., Parfenov V. A., Knyazeva A. D., Mitryashkin A. N., Replyanski N., Kasyanov V. A., Pereira F.: Patterning of tissue spheroids biofabricated from human fibroblasts on the surface of electrospun polyurethane matrix using 3D bioprinter. International Journal of Bioprinting, **2**, 45–52 (2016). https://doi.org/10.18063/IJB.2016.01.007

[16] Efimov A. E., Agapova O. I., Safonova L. A., Bobrova M. M., Parfenov V. A., Koudan E. V., Pereira F. D. A. S., Bulanova E. A., Mironov V. A., Agapov I. I.: Nanostructural features of contacts of fibroblasts with dual-scale biocompatible polyurethane scaffold. Nanotechnologies in Russia, **11**, 830–834 (2016). https://doi.org/10.1134/S1995078016060094

[17] Appel A. A., Anastasio M. A., Larson J. C., Brey E. M.: Imaging challenges in biomaterials and tissue engineering. Biomaterials, **34**, 6615–6630 (2013). https://doi.org/10.1016/j.biomaterials.2013.05.033

[18] Al-Abboodi A., Fu J., Doran P. M., Chan P. O. Y.: Three-dimensional nanocharacterization of porous hydrogel with ion and electron beams. Biotechnology and Bioengineering, **110**, 318–326 (2013). https://doi.org/10.1002/bit.24612

[19] Stachewicz U., Qiao T., Rawlinson S. C. F., Almeida F. V., Li W-Q., Cattell M., Barber A. H.: 3D imaging of cell interactions with electrospun PLGA nanofiber membranes for bone regeneration. Acta Biomaterialia, **27**, 88–100 (2015). https://doi.org/10.1016/j.actbio.2015.09.003

[20] Bradley R. S., Robinson I. K., Yusuf M.: 3 3D X-ray nanotomography of cells grown on electrospun scaffolds. Macromolecular Bioscience, **17**, 1600236/1–1600236/8 (2017). https://doi.org/10.1002/mabi.201600236

[21] Yang Y., Heine R., Cheng Y., Wang C-C., Song Y-F., Baumbach T.: Approaching quantitative Zernike phase contrast in full-field transmission hard X-ray microscopy: Origin and reduction of artifacts. Applied Physics Letters, **105**, 094101/1–094101/5 (2014). https://doi.org/10.1063/1.4894276

[22] Langer M., Peyrin F.: 3D X-ray ultra-microscopy of bone tissue. Osteoporosis International, **27**, 441–455 (2016). https://doi.org/10.1007/s00198-015-3257-0

[23] Bailey R. J., Geurts R., Stokes D. J., de Jong F., Barber A. H.: Evaluating focused ion beam induced damage in soft materials. Micron, **50**, 51–56 (2013). https://doi.org/10.1016/j.micron.2013.04.005

[24] Caplan J., Niethammer M., Taylor R. M. II, Czymmek K. J.: The power of correlative microscopy: Multimodal, multi-scale, multi-dimensional. Current Opinion in Structural Biology, **21**, 686–693 (2011). https://doi.org/10.1016/j.sbi.2011.06.010

[25] Alekseev A., Efimov A., Loos J., Matsko N., Syurik J.: Three-dimensional imaging of polymer materials by scanning probe tomography. European Polymer Journal, **52**, 154–165 (2014). https://doi.org/10.1016/j.eurpolymj.2014.01.003

[26] Alekseev A., Chen D., Tkalya E. E., Ghislandi M. G., Syurik Y., Ageev O., Loos J., de With G.: Local organization of graphene network inside graphene/polymer composites. Advanced Functional Materials, **22**, 1311–1318 (2012). https://doi.org/10.1002/adfm.201101796

[27] Efimov A. E., Moisenovich M. M., Bogush V. G., Agapov I. I.: 3D nanostructural analysis of silk fibroin and recombinant spidroin 1 scaffolds by scanning probe nanotomography. RSC Advances, **4**, 60943–60947 (2014). https://doi.org/10.1039/C4RA08341E

[28] Mattila P. K., Lappalainen P.: Filopodia: Molecular architecture and cellular functions. Nature Reviews Molecular Cell Biology, **9**, 446–454 (2008). https://doi.org/10.1038/nrm2406

[29] Xue F., Janzen D. M., Knecht D. A.: Contribution of filopodia to cell migration: A mechanical link between protrusion and contraction. International Journal of Cell Biology, **2010**, 507821/1–507821/13 (2010). https://doi.org/10.1155/2010/507821

[30] Eida S., van Cauteren M., Hotokezaka Y., Katayama I., Sasaki M., Obara M., Okuaki T., Sumi M., Nakamura T.: Length of intact plasma membrane determines the diffusion properties of cellular water. Scientific Reports, **6**, 19051/1–19051/12 (2016). https://doi.org/10.1038/srep19051

[31] Efimov A. E., Agapova O. I., Safonova L. A., Bobrova M. M., Volkov A. D., Khamkhash L., Agapov I. I.: Cryo scanning probe nanotomography study of the structure of alginate microcarriers. RSC Advances, **7**, 8808–8815 (2017). https://doi.org/10.1039/C6RA26516B

[32] Keren K., Pincus Z., Allen G. M., Barnhart E. L., Marriott G., Mogilner A., Theriot J. A.: Mechanism of shape determination in motile cells. Nature, **453**, 475–481 (2008). https://doi.org/10.1038/nature06952

[33] Krobath H., Schütz G. J., Lipowsky R., Weikl T. R.: Lateral diffusion of receptor-ligand bonds in membrane adhesion zones: Effect of thermal membrane roughness. Europhysics Letters, **78**, 38003/1–38003/6 (2007). https://doi.org/10.1209/0295-5075/78/38003

[34] Reister E., Bihr T., Seifert U., Smith A-S.: Two intertwined facets of adherent membranes: Membrane roughness and correlations between ligand–receptors bonds. New Journal of Physics, **13**, 025003/1–025003/15 (2011). https://doi.org/10.1088/1367-2630/13/2/025003

[35] Antonio P. D., Lasalvia M., Perna G., Capozzi V.: Scale-independent roughness value of cell membranes studied by means of AFM technique. Biochimica et Biophysica Acta (BBA) - Biomembranes, **1818**, 3141–3148 (2012). https://doi.org/10.1016/j.bbamem.2012.08.001

[36] Lee H., Veerapandian M., Kim B. T., Yun K., Seo S-W.: Functional nanoparticles translocation into cell and adhesion force curve analysis. Journal of Nanoscience and Nanotechnology, **12**, 7752–7763 (2012). https://doi.org/10.1166/jnn.2012.6596

[37] Wang Y., Xu C., Jiang N., Zheng L., Zeng J., Qiu C., Yang H., Xie S.: Quantitative analysis of the cell-surface roughness and viscoelasticity for breast cancer cells discrimination using atomic force microscopy. Scanning, **38**, 558–563 (2016). https://doi.org/10.1002/sca.21300

[38] Staykova M., Holmes D. P., Read C., Stone H. A.: Mechanics of surface area regulation in cells examined with confined lipid membranes. PNAS, **108**, 9084–9088 (2011). https://doi.org/10.1073/pnas.1102358108

[39] Sheets K., Wunsch S., Ng C., Nain A. S.: Shape-dependent cell migration and focal adhesion organization on suspended and aligned nanofiber scaffolds. Acta Biomaterialia, **9**, 7169–7177 (2013). https://doi.org/10.1016/j.actbio.2013.03.042

[40] Kennedy K. M., Bhaw-Luximon A., Jhurry D.: Cell-matrix mechanical interaction in electrospun polymeric scaffolds for tissue engineering: Implications for scaffold design and performance. Acta Biomaterialia, **50**, 41–55 (2017). https://doi.org/10.1016/j.actbio.2016.12.034

[41] Balashov V., Efimov A., Agapova O., Pogorelov A., Agapov I., Agladze K.: High resolution 3D microscopy study of cardiomyocytes on polymer scaffold nanofibers reveals formation of unusual sheathed structure. Acta Biomaterialia, **68**, 214–222 (2018). https://doi.org/10.1016/j.actbio.2017.12.031

[42] Serra T., Mateos-Timoneda M. A., Planell J. A., Navarro M.: 3D printed PLA-based scaffolds. Organogenesis, **9**, 239–244 (2013). https://doi.org/10.4161/org.26048

[43] Koch B., Meyer A. K., Helbig L., Harazim S. M., Storch A., Sanchez S., Schmidt O. G.: Dimensionality of rolled-up nanomembranes controls neural stem cell migration mechanism. Nano Letters, **15**, 5530–5538 (2015). https://doi.org/10.1021/acs.nanolett.5b02099

[44] Bosworth L. A., Turner L-A., Cartmell S. H.: State of the art composites comprising electrospun fibres coupled with hydrogels: A review. Nanomedicine: Nanotechnology, Biology, and Medicine, **9**, 322–335 (2013). https://doi.org/10.1016/j.nano.2012.10.008

[45] Ando T., Uchihashi T., Kodera N.: High-speed AFM and applications to biomolecular systems. Annual Review of Biophysics, **42**, 393–414 (2013). https://doi.org/10.1146/annurev-biophys-083012-130324

[46] Efimov A. E., Agapov I. I., Agapova O. I., Oleinikov V. A., Mezin A. V., Molinari M., Nabiev I., Mochalov K. E.: A novel design of a scanning probe microscope integrated with an ultramicrotome for serial block-face nanotomography. Review of Scientific Instruments, **88**, 023701/1–023701/6 (2017). https://doi.org/10.1063/1.4975202

[47] Efimov A. E., Bobrovsky A. Y., Agapov I. I., Agapova O. I., Oleinikov V. A., Nabiev I. R., Mochalov K. E.: Scanning near-field optical nanotomography: A new method of multiparametric 3D investigation of nanostructural materials. Technical Physics Letters, **42**, 171–174 (2016). https://doi.org/10.1134/S1063785016020231